Electronic Supplementary Information

Precursor Salt Assisted Syntheses of High-Index Faceted Concave Hexagon and Nanorod like Polyoxometalates

Jaya Pal,[a] Mainak Ganguly,[a] Chanchal Mondal,[a] Yuichi Negishi[b] and Tarasankar Pal[a]*

[a]Department of Chemistry, Indian Institute of Technology, Kharagpur-721302, India

[b]Department of Applied Chemistry, Tokyo University of Science, Tokyo 1628601, Japan

E-mail: tpal@chem.iitkgp.ernet.in

Chemicals

All the chemicals were of analytical grade. Double-distilled water was used throughout the course of experiments. $Cu(CH_3COO)_2.H_2O$, $CuSO_4.5H_2O$, $CuCl_2.2H_2O$ and $Cu(NO_3)_2.3H_2O$, $[(NH_4)_6Mo_7O_{24}.4H_2O]$, Na_2MoO_4, ammonia, ammonium acetate and Congo red was purchased from E-Merck. All glassware was properly cleaned and dried well before use.

Analytical Instruments

Powder X-ray diffraction (XRD) was carried out with a PW-1710 X-ray diffractometer (40 kV, 20 mA) with Cu Kα radiation (λ = 1.5418 A) at a scanning rate of 0.5° min^{-1}. All XRD data were analyzed by using (JCPDS) software.

X-ray photoelectron spectroscopy (XPS) analysis was performed with a VG Scientific ESCALAB MK II spectrometer (UK) equipped with Mg Kα excitation source (1253.6 eV) and a five-channeltron detection system to authenticate the elemental state.

Field emission scanning electron microscopy (FESEM) was performed with a Supra 40, Carl Zeiss Pvt. Ltd.

Transmission electron microscopy (TEM) was carried out on a Hitachi H-9000 NAR instrument, operating at 100 kV on a carbon coated copper grid.

Energy dispersive X-ray (EDX) analysis was done with an Oxford link and ISIS 300 instruments.

All UV-vis absorption spectra were recorded on SPECTRASCAN UV 2600 digital spectrophotometer (Chemito, India) and absorbance was measured by taking all solutions in a 1cm well stoppard quartz cuvette.

The Brunauer-Emmett-Teller (BET) surface area and pore size distribution were measured with an ASAP 2020 V3.01 G from N_2 adsorption-desorption isotherms.

HRTEM Analysis

Fig. S8, ESI shows the HRTEM images of morphologically different ACM and CMOH microstructures. Hexagonal plate like ACM exhibits fringe spacing value of 0.72 and 0.52 nm which are consistent with the {001} and {010} crystal planes (Fig. S8a, b, ESI). As measured from the Fig. S8c, ESI, fringe spacing value of circular plate like ACM is 0.51 nm indicating {101} crystal plane of ACM. Flower like ACM shows the fringe spacing value of 0.307 nm which coincides with $\{1\bar{1}1\}$ crystal plane of ACM (Fig. S8d, ESI). HRTEM image (Fig. S8e, ESI) of concave hexagonal plate like ACM depicts fringe spacing value 0.151 nm which coincides with the high index {422} crystal plane. Fig. S8f, ESI reveals the fringe spacing value of prickly spherical CMOH is 0.415 nm which indicates $\{\bar{1}01\}$ directional growth of prickly spherical CMOH. CMOH nanorod exhibits fringe spacing value of 0.345 nm which confirms that the nanorods grow along the {111} direction (Fig. S8g, ESI).

BET Measurements of ACMs and CMOHs

To have a comparative account of surface area and porosity of differently shaped ACMs and CMOHs, BET experiment has been performed (Fig. S9a-f, ESI). The BET surface area values of the hexagonal plate, circular plate, hollow flower, and concave hexagonal plate like

ACMs are 2.091, 2.487, 18.702, and 5.804 m^2/g, respectively (Fig. S9a-d, ESI). The pore volumes of the ACMs are 0.0118, 0.0082, 0.0707, and 0.0186 cc/g, respectively. The photodegradation performance of differently shaped ACMs towards congo red degradation follows the sequence: concave hexagon > hollow flower > hexagonal plate > circular plate and the order is not in good agreement with the BET surface area. But the exposed facet from the HRTEM measurement strongly supports their relative catalytic performances. Interestingly concave hexagonal plate like ACM exhibit highest catalytic activity due to the promotional effect of high index facet. The BET surface area values of the prickly sphere, and rod like CMOHs are 38.123, and 41.486 m^2/g, respectively (Fig. S9e,f, ESI). The pore volumes of the CMOHs are 0.112, and 0.121 cc/g respectively. As the surface area values are almost comparable, so higher photocatalytic activity of rod like CMOH compared to prickly sphere cannot be accounted again in terms of BET surface area measurements. So the results support the facet dependent photocatalytic activity towards congo red degradation.

SAED, EDX and Area Mapping

Fig. S13a-f, ESI shows the selected area electron diffraction (SAED) patterns of the surface region of morphologically different ACMs (hexagonal plate, circular plate, hollow flower and concave hexagonal plate) and CMOHs (prickly sphere and rod), respectively. All the SAED patterns demonstrate the appearance of very sharp diffraction spots, which, in turn, specify the formation of well-developed single-crystalline ACM and CMOH with different morphologies.

The composition of all five morphologically different ACM and CMOH microstructures were further studied by energy dispersive X-ray spectroscopic (EDX) analysis (Fig. S14a-f, ESI) and area mapping (Fig. S15 and S16, ESI). Area mappings of all three morphologically different ACM microstructures suggest the presence of four elements such as Cu, Mo, O and N (Fig. S15, ESI). From each area mapping, it is observed that all four elements are

homogeneously distributed over the whole matrix. Area mappings of prickly sphere and rod like CMOH microstructures imply the presence of three elements such as Cu, Mo and O (Fig. S16, ESI). From each area mapping, it is found that all three elements are homogeneously distributed over the whole matrix.

Table S2a, ESI depicts the weight % values of Cu, Mo and N for hexagonal plate, circular plate, hollow flower, and concave hexagonal plate like ACMs. Again the weight % values of Cu and Mo for prickly sphere, and rod like CMOHs are presented in Table S2b, ESI. We observed that the values obtained from EDX analysis are in close proximity with the calculated values.

Figure, Scheme and Table

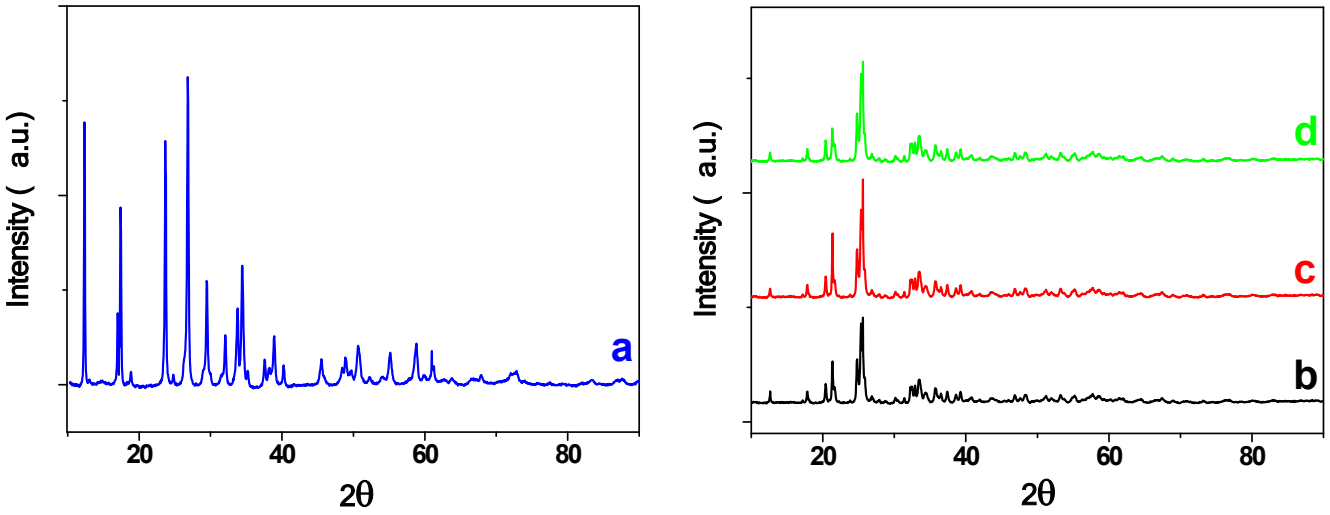

Fig. S1 Curve a shows the XRD pattern of concave hexagonal plate like ACM microstructure. Curves b-d show the XRD patterns of CMOH nanorods obtained from CA assisted reaction of hexagonal plate, circular plate and hollow flower like ACM microstructures, respectively.

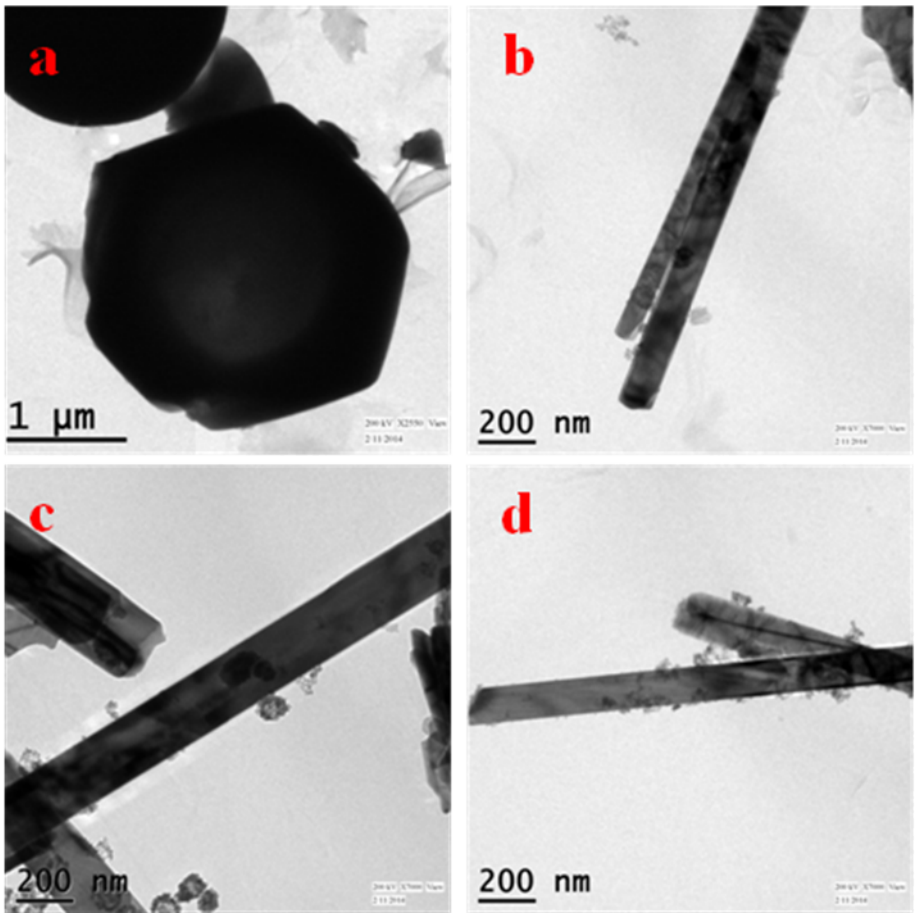

Fig. S2 TEM images of (a) concave hexagonal plate like ACM microstructure. TEM images (b-d) of rod like CMOH obtained from CA assisted reaction of hexagonal plate, circular plate and hollow flower like ACM microstructures, respectively.

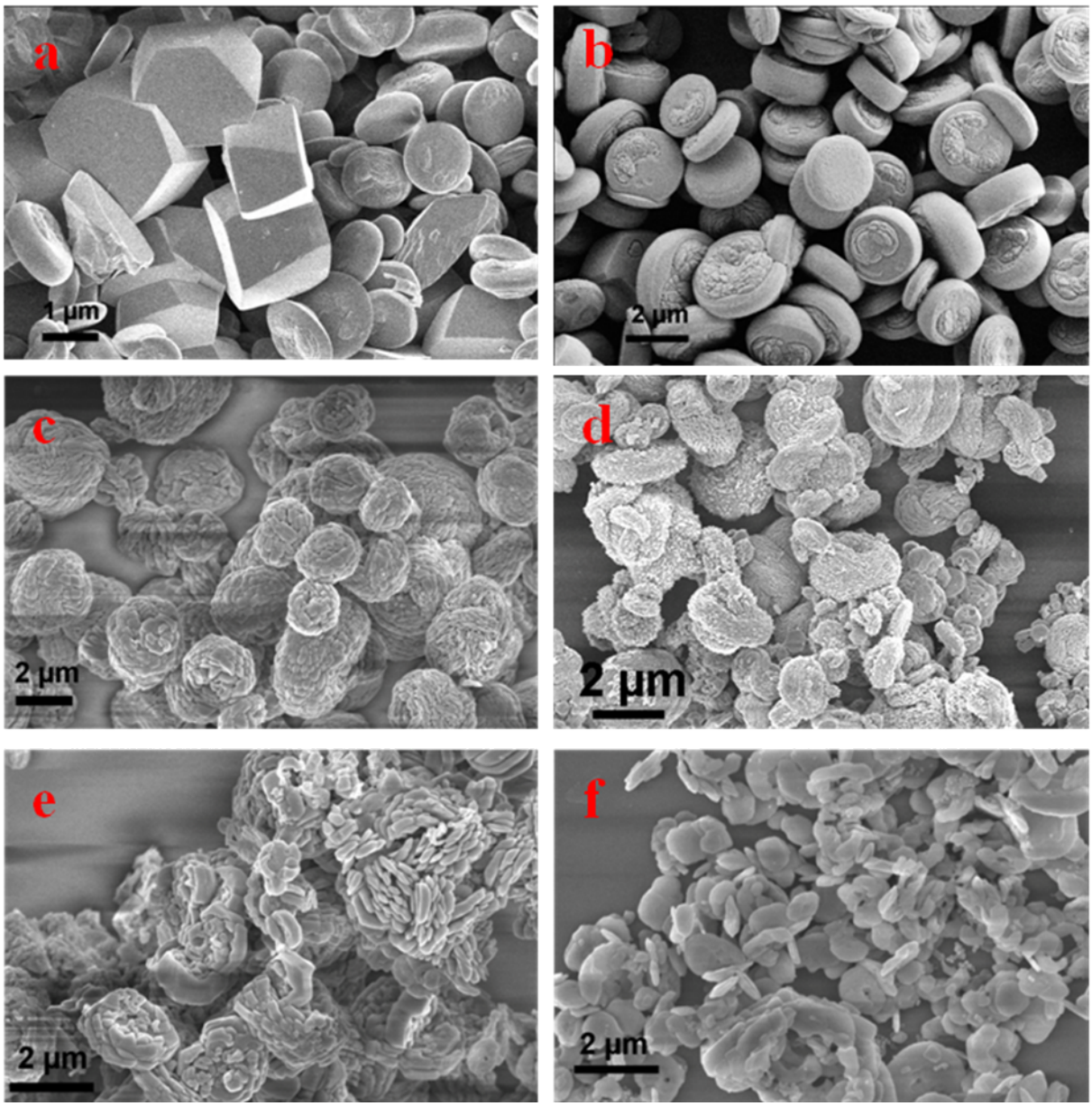

Fig. S3 FESEM images of as-synthesized ACM microstructures obtained from different precursor ratios of CA and AHM (a) 1.5:8.5, (b) 2.5:7.5, (c) 4:6, (d) 5:5, (e) 6: 4 and (f) 7:3 respectively under MHT condition for 12h.

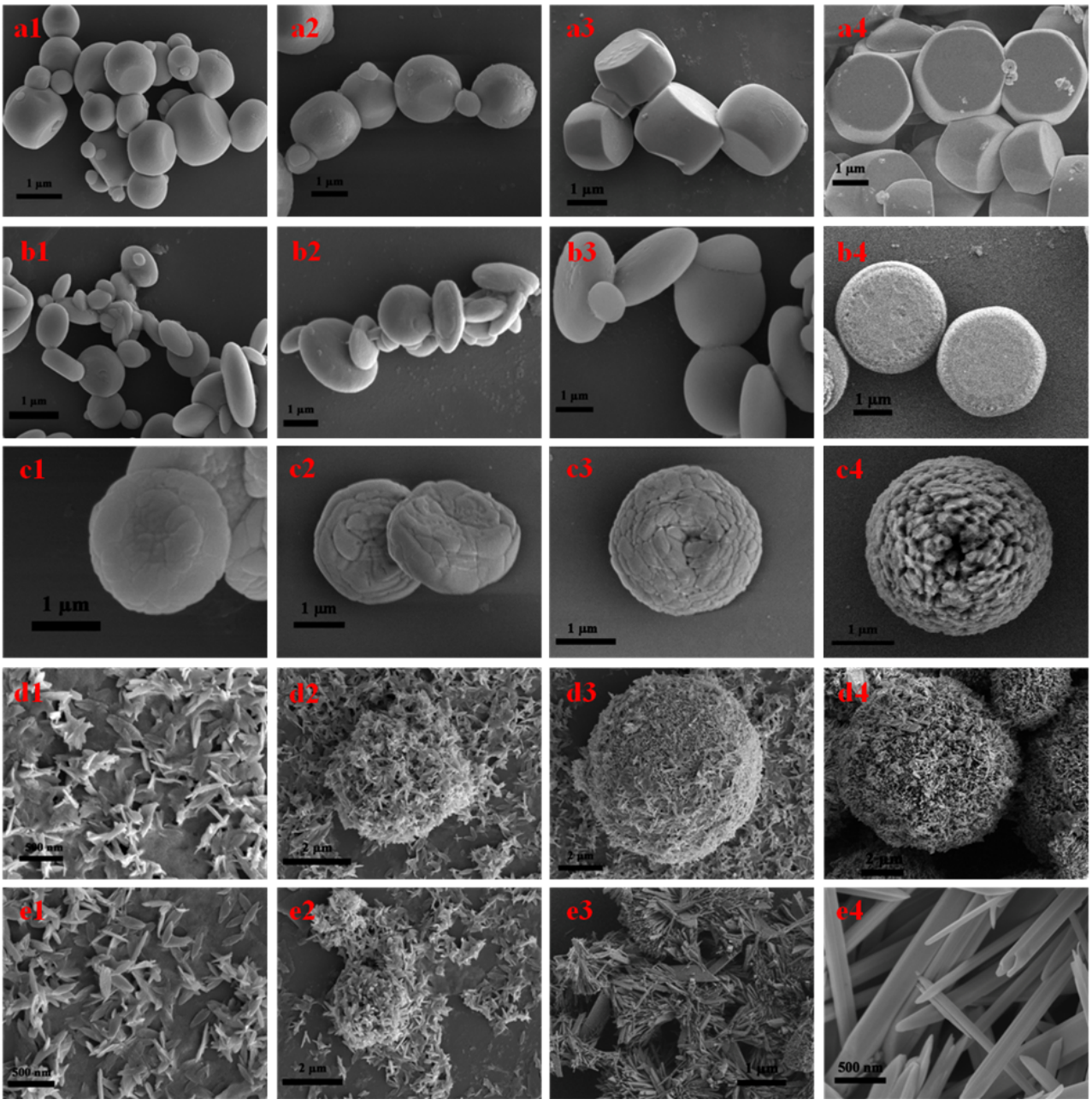

Fig. S4 Time dependent FESEM images for the formation of (a4) hexagonal plate, (b4) circular plate and (c4) hollow flower like ACM microstructures and (d4) prickly sphere and (e4) rod like CMOH microstructures, respectively. (a1, b1, c1, d1 and e1), (a2, b2, c2, d2 and e2), (a3, b3, c3, d3 and e3) and (a4, b4, c4, d4 and e4) are the products obtained after different time intervals such as 1, 4, 8 and 12 h reaction, respectively.

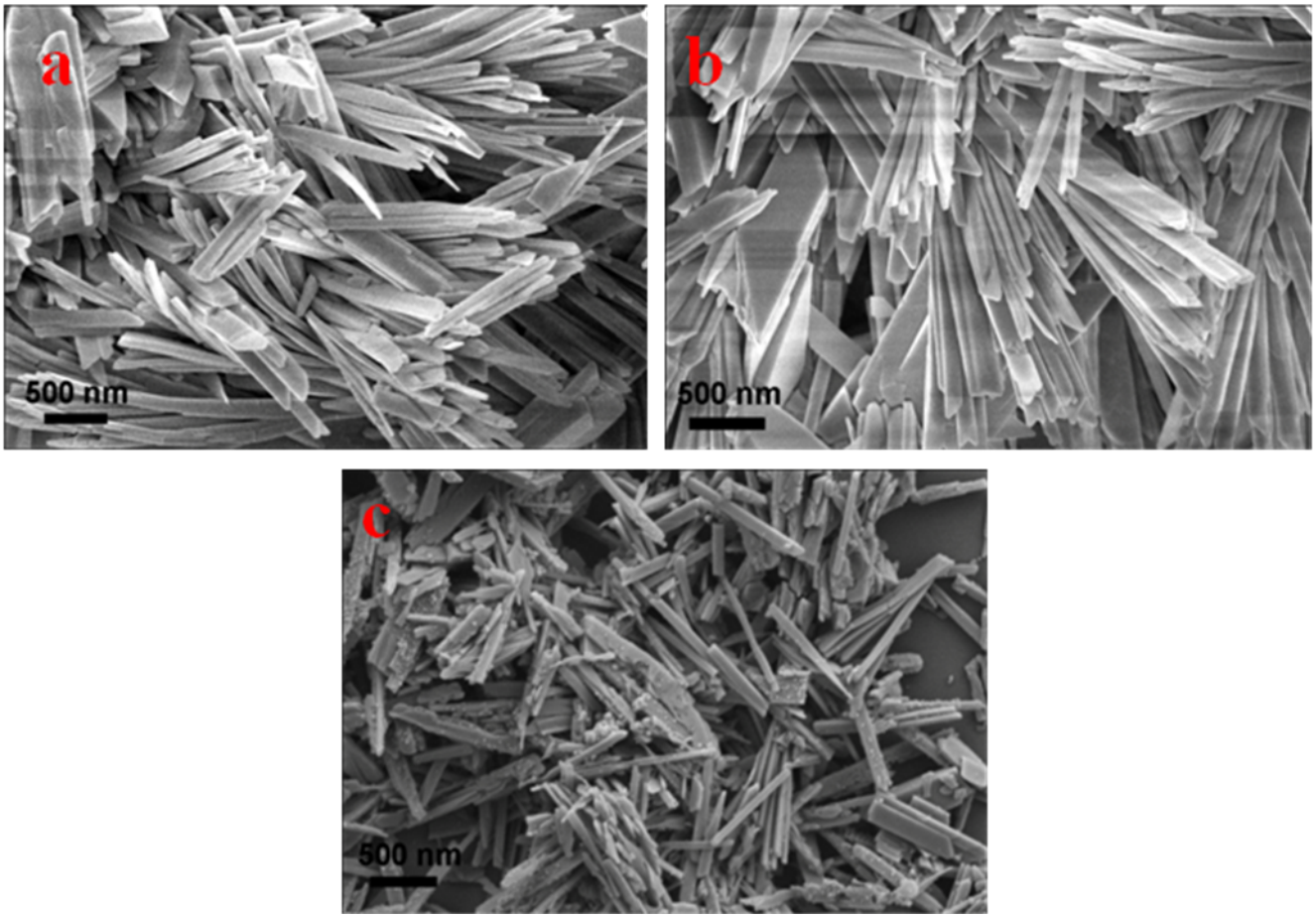

Fig. S5 FESEM images of as-synthesized CMOH nanorods obtained from individual reaction of hexagonal plate like ACM with (a) $CuSO_4$, (b) $CuCl_2$ and (c) $Cu(NO_3)_2$, respectively under MHT condition for 12h.

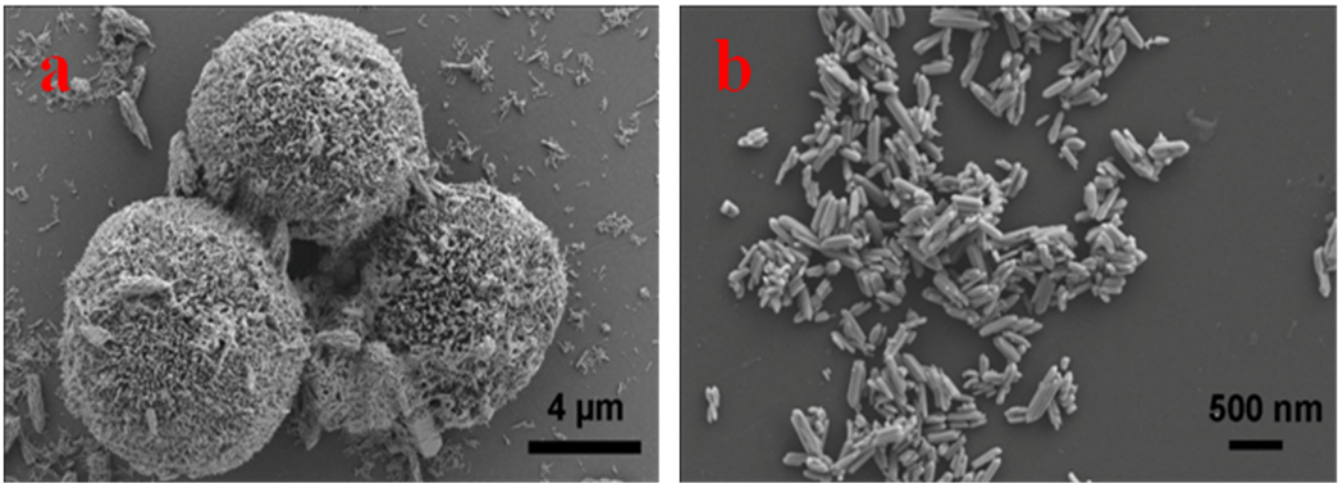

Fig. S6 FESEM images of as-synthesized CMOH products obtained after treatment of hexagonal ACM with (a) low (0.01 M) and (b) high (0.1 M) concentration of CA solution respectively.

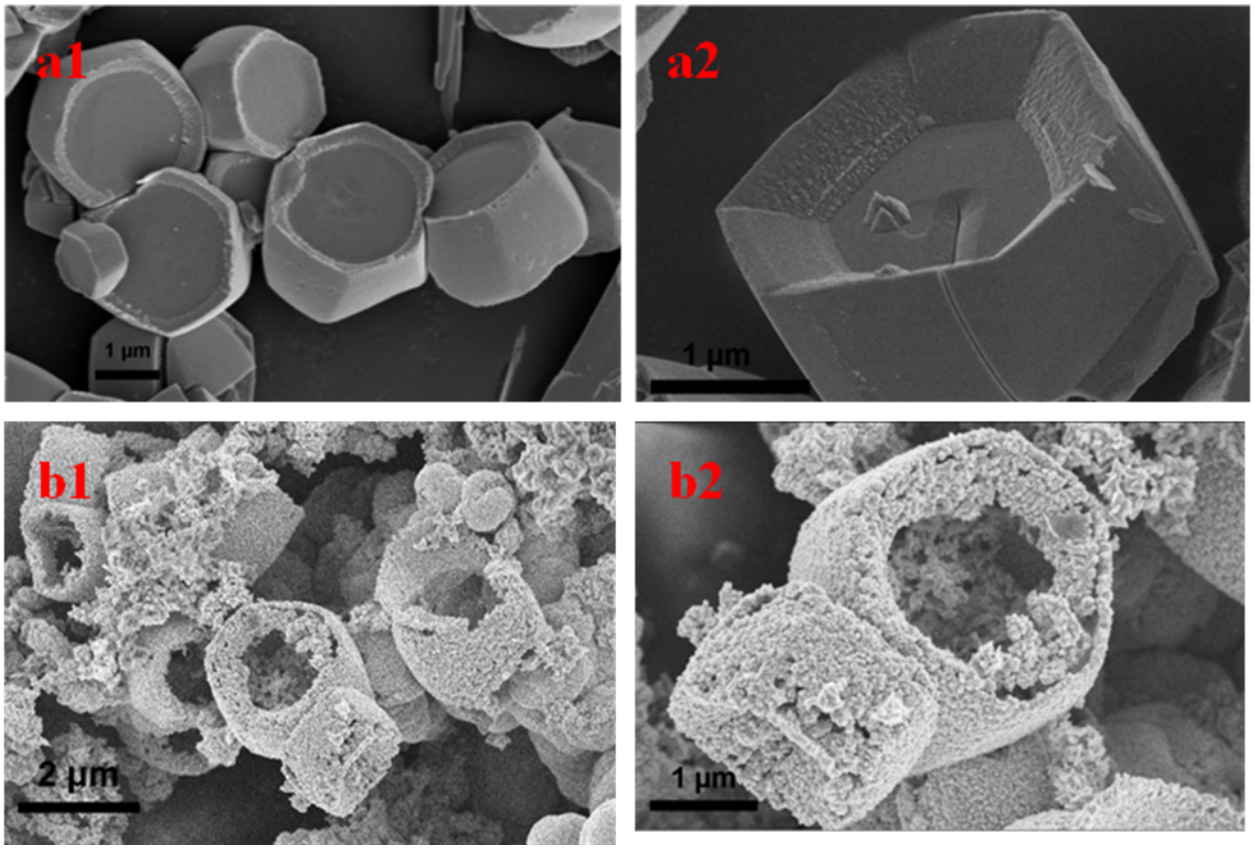

Fig. S7 FESEM images of as-obtained products when hexagonal plate like ACM treated with (a1 and a2) ammonium acetate and (b1 and b2) ammonium solution, respectively.

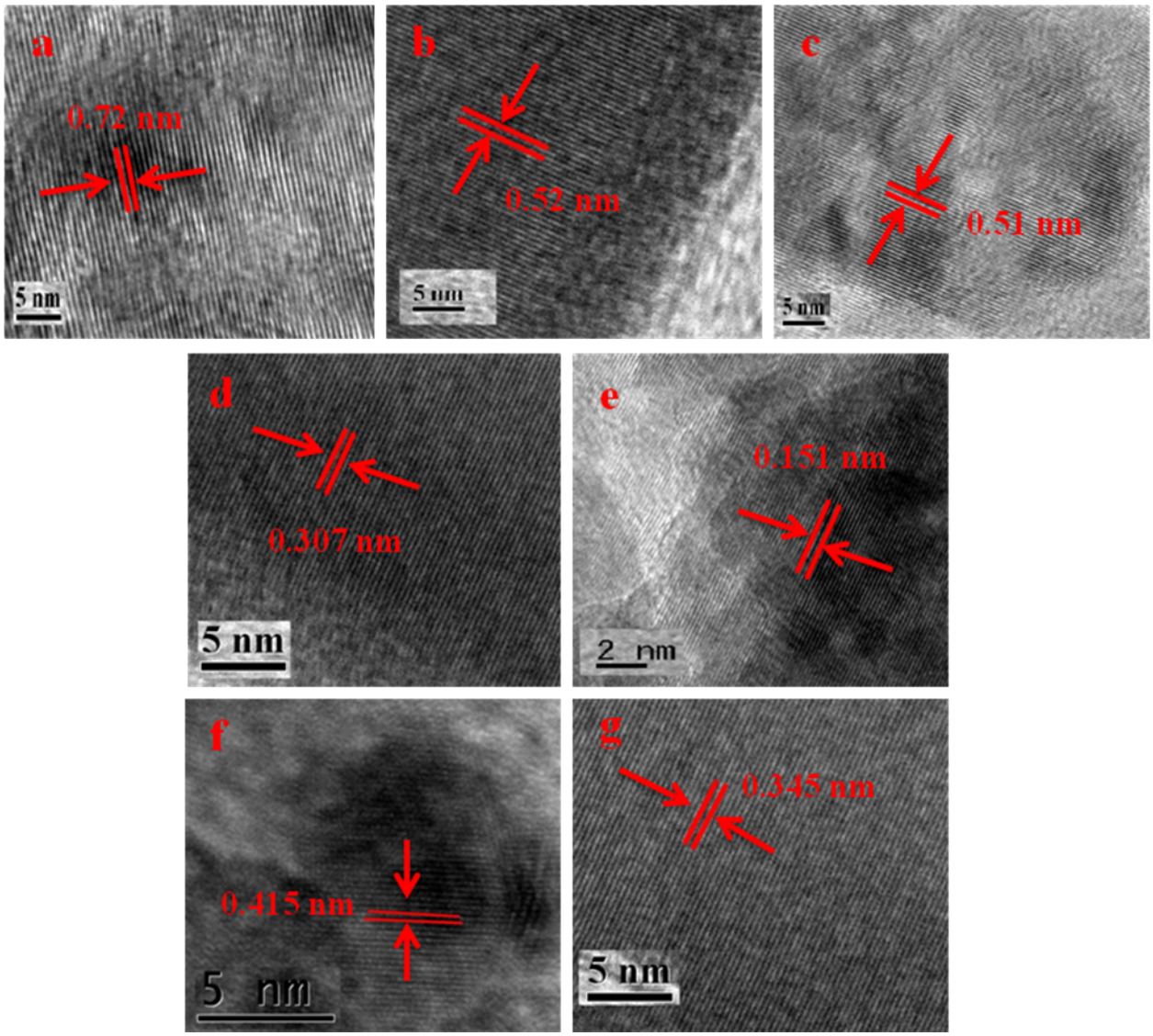

Fig. S8 HRTEM images of as-synthesized (a, b) hexagonal plate, (c) circular plate, (d) hollow flower, and (e) concave hexagonal plate like ACM microstructures, respectively. HRTEM images of as-obtained (f) prickly sphere and (g) rod like CMOH, respectively.

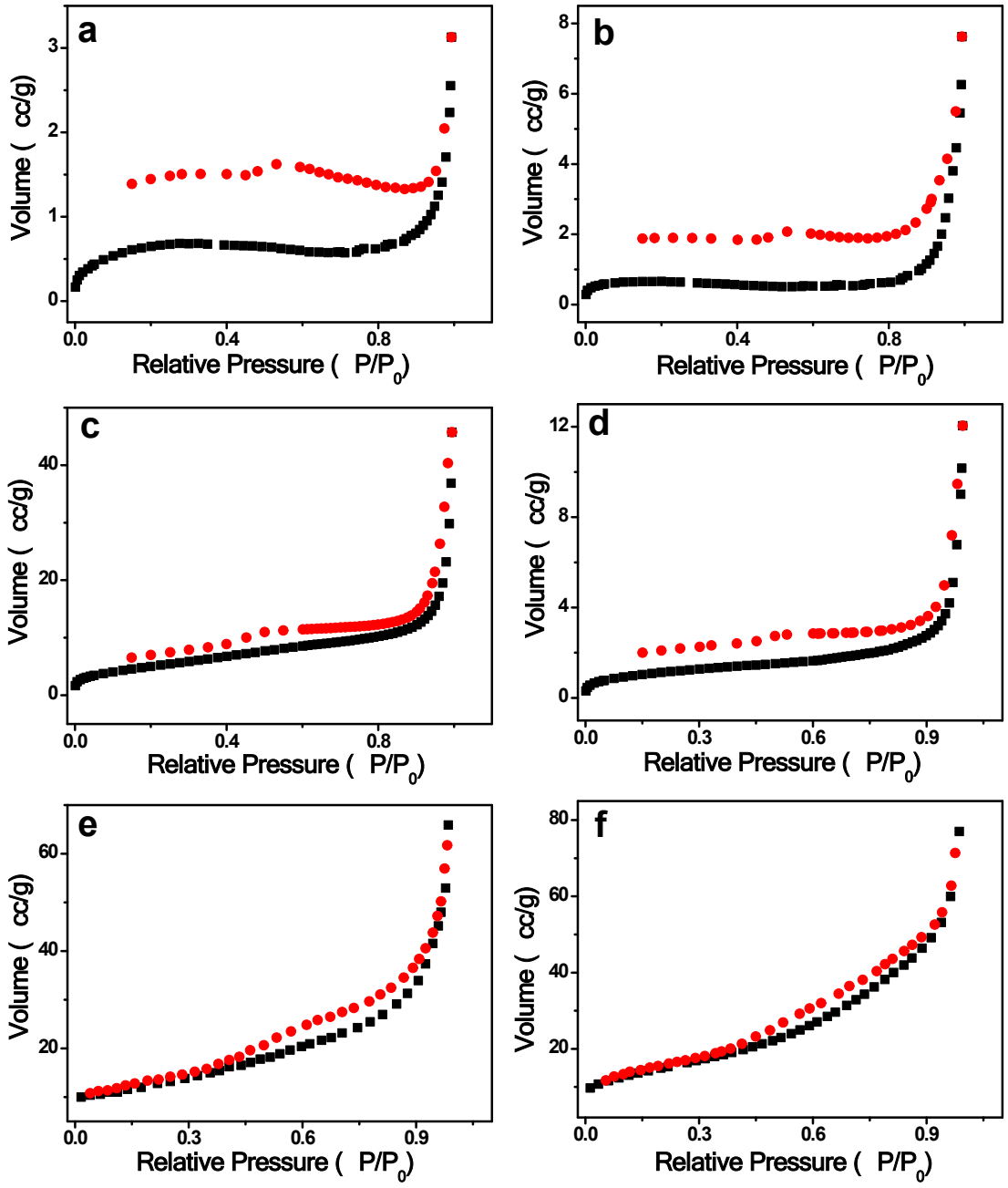

Fig. S9 Nitrogen adsorption-desorption isotherm of (a) hexagonal plate, (b) circular plate, (c) hollow flower, and (d) concave hexagonal plate like ACM microstructures and (e) prickly sphere and (f) rod like CMOH microstructures.

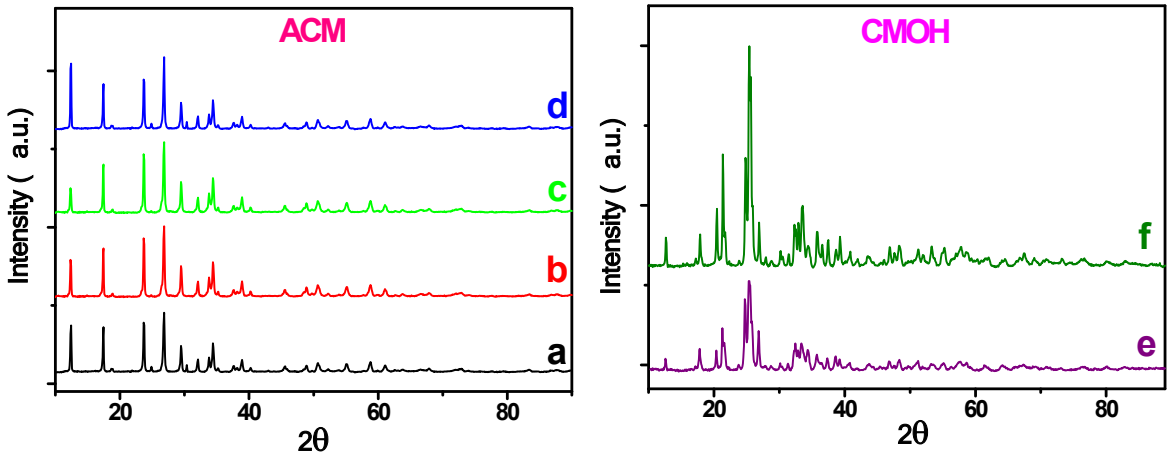

Fig. S10 Curves a-d show the XRD patterns of hexagonal plate, circular plate, hollow flower and concave hexagonal plate like ACM microstructures, respectively after the 4thcatalytic cycle. Curves e and f depict the XRD patterns of prickly sphere and rod like CMOH microstructures, respectively after the 4thcatalytic cycle.

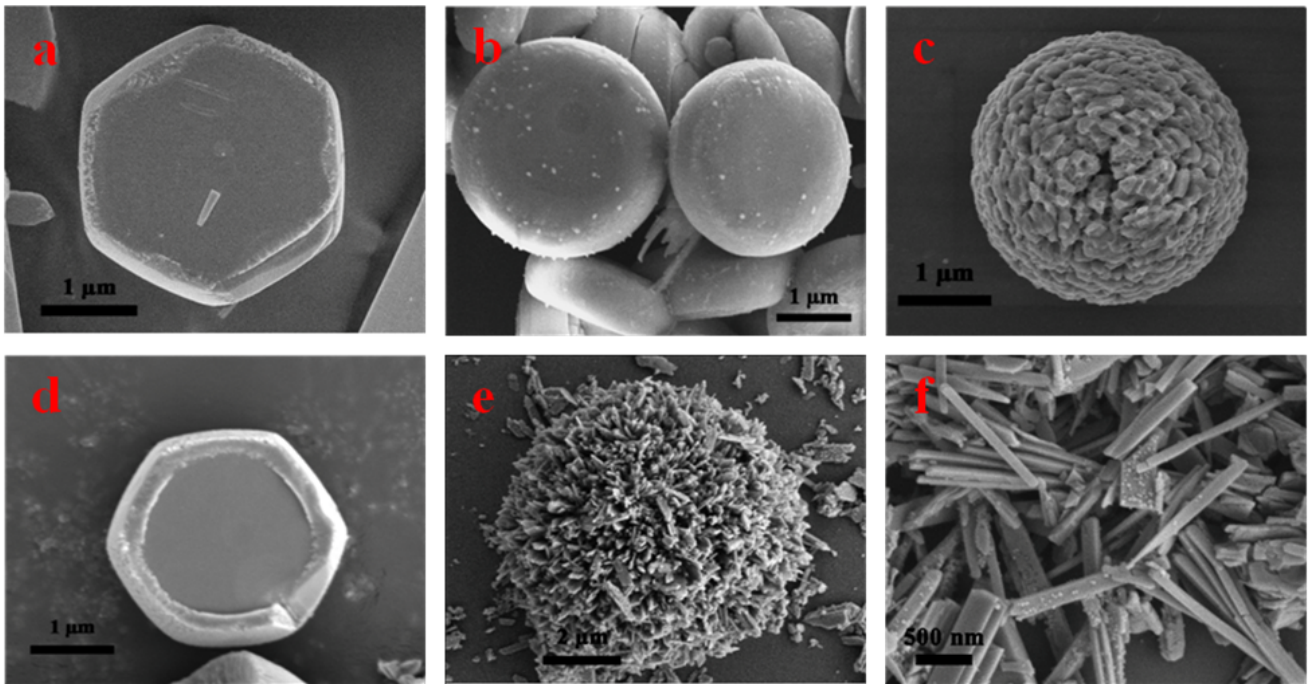

Fig. S11 High magnification FESEM images of (a) hexagonal plate, (b) circular plate, (c) hollow flower and (d) concave hexagonal plate like ACM microstructures and (e) prickly sphere and (f) rod like CMOH microstructures, respectively after the 4th catalytic cycle.

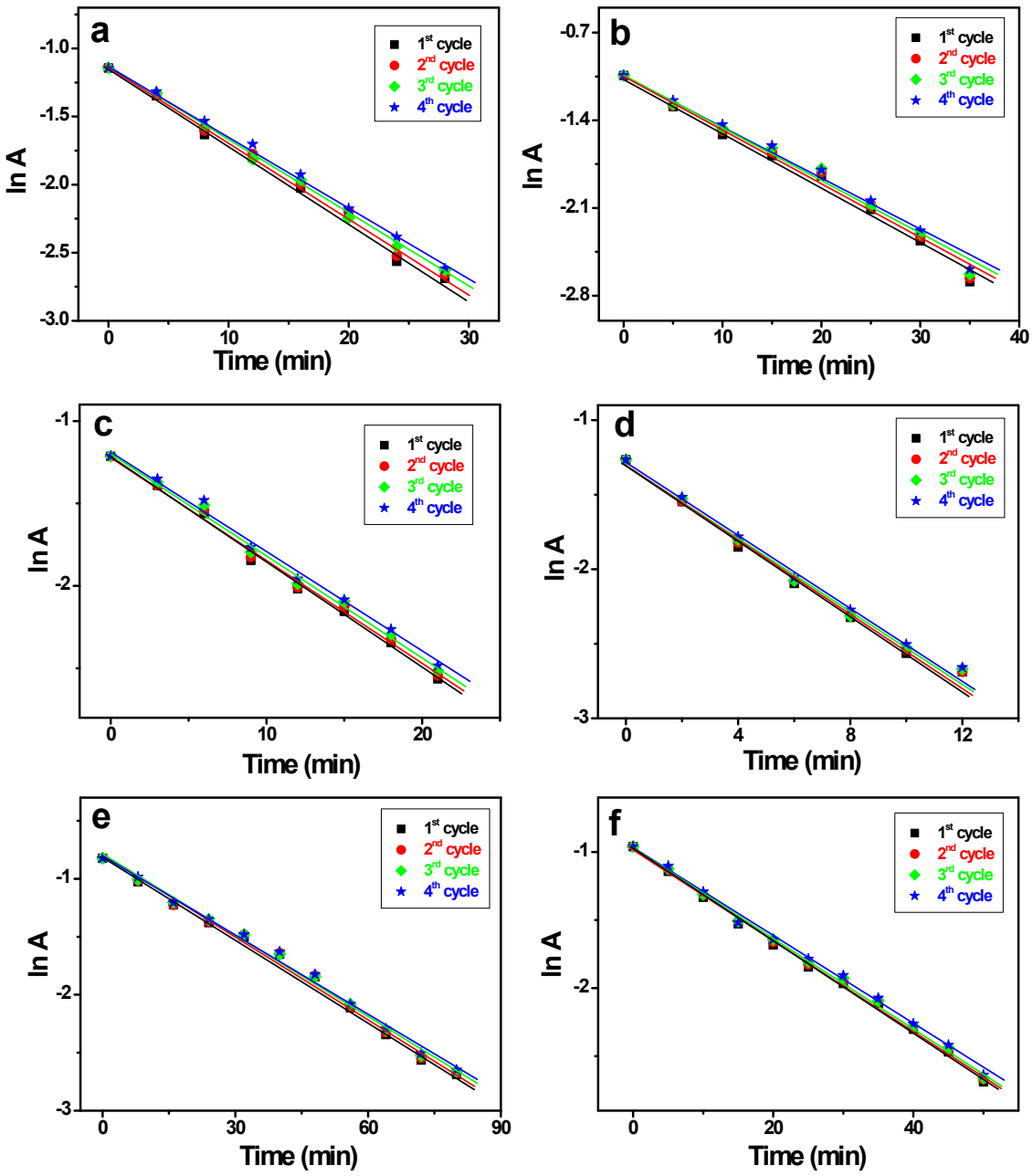

Fig. S12 lnA vs time plot for degradation of congo red solution at different cycles by using (a) hexagonal plate, (b) circular plate, (c) hollow flower and (d) concave hexagonal plate like ACM microstructures and (e) prickly sphere and (f) rod like CMOH microstructures as catalyst.

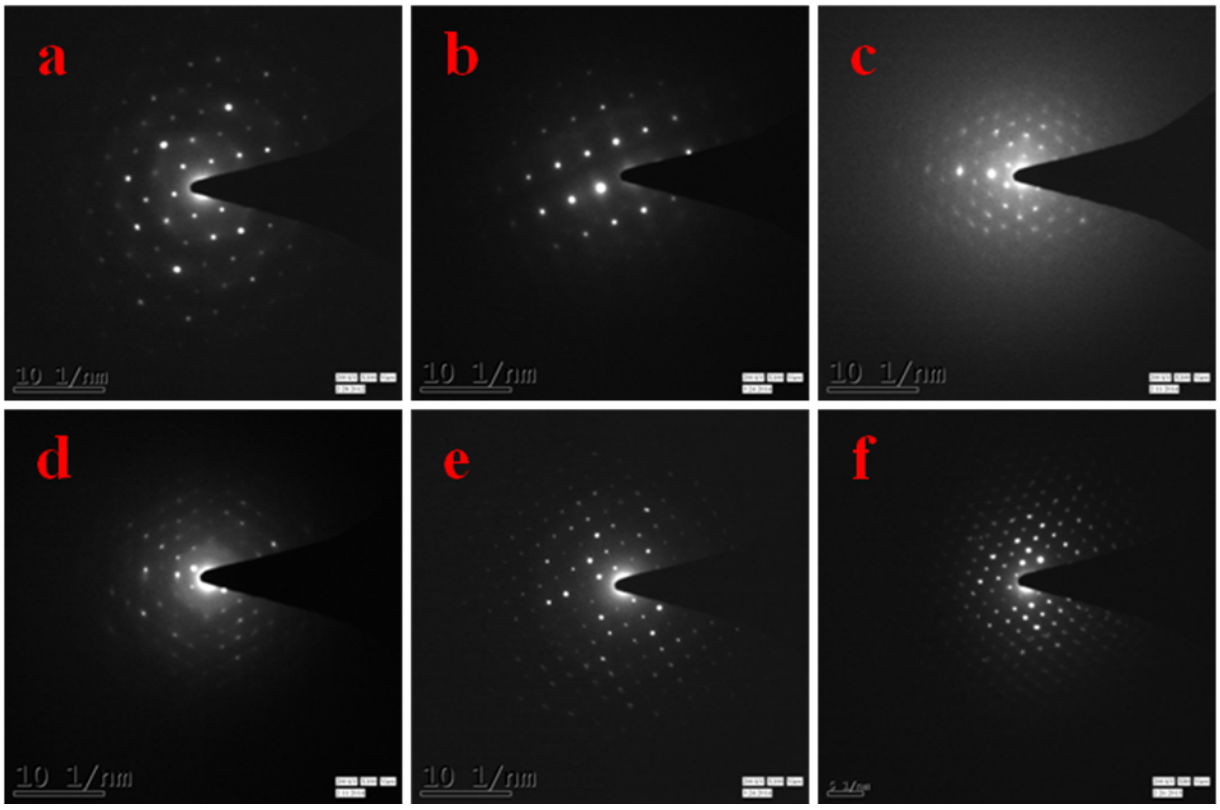

Fig. S13 SAED patterns of as- obtained (a) hexagonal plate, (b) circular plate, (c) hollow flower, and (d) concave hexagonal plate like ACM microstructures, respectively. SAED patterns of as-synthesized (e) prickly sphere and (f) rod like CMOH, respectively.

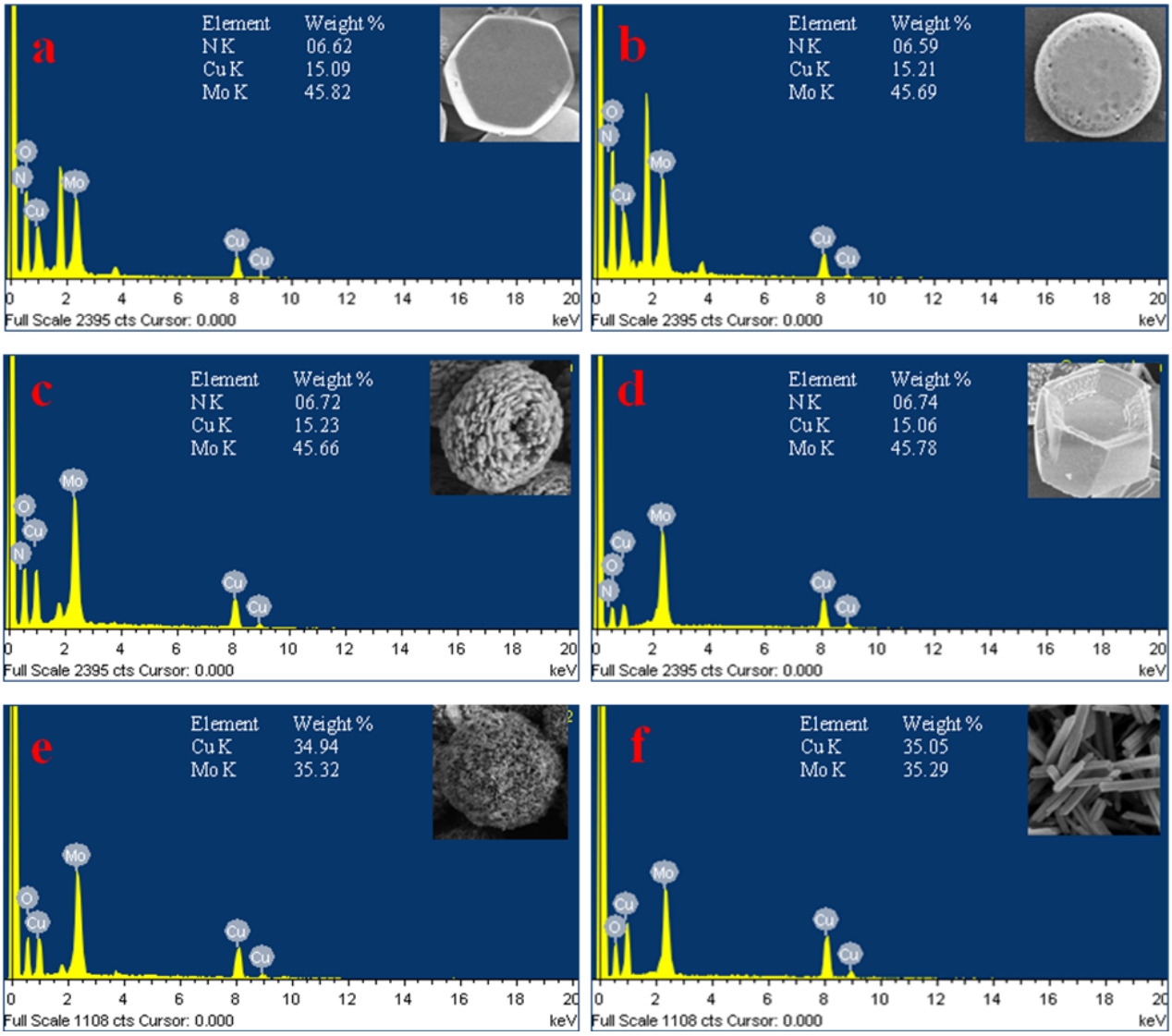

Fig. S14 EDX analysis of as-synthesized (a) hexagonal plate, (b) circular plate, (c) hollow flower, and (d) concave hexagonal plate like ACM microstructures, respectively. EDX analysis of as-synthesized (e) prickly sphere and (f) rod like CMOH, respectively.

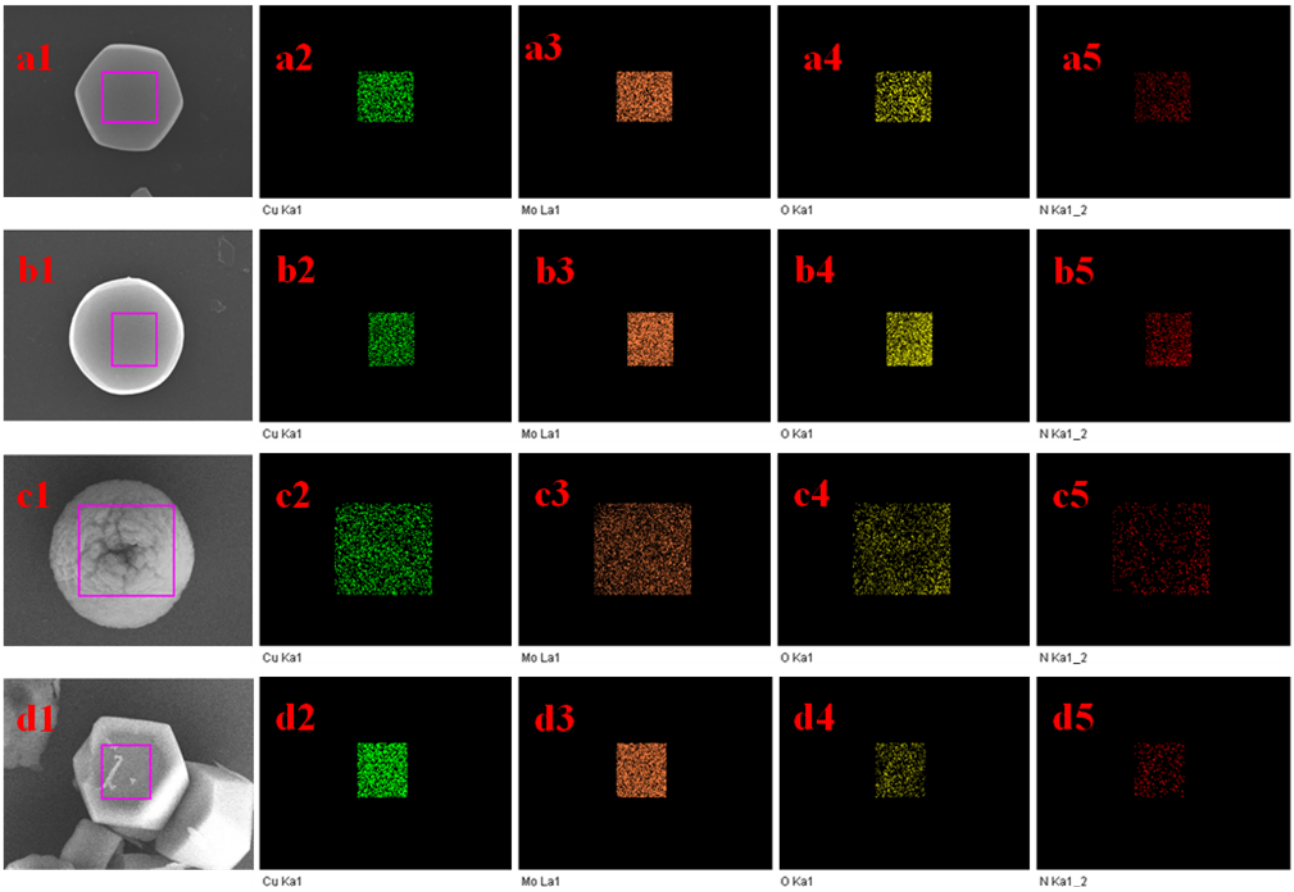

Fig. S15 Area mapping of as-synthesized (a1) hexagonal plate, (b1) circular plate, (c1) hollow flower, and (d1) concave hexagonal plate like ACM microstructures: for the element Cu (a2, b2, c2 and d2), Mo (a3, b3, c3 and d3), O (a4, b4, c4 and d4) and N (a5, b5, c5 and d5).

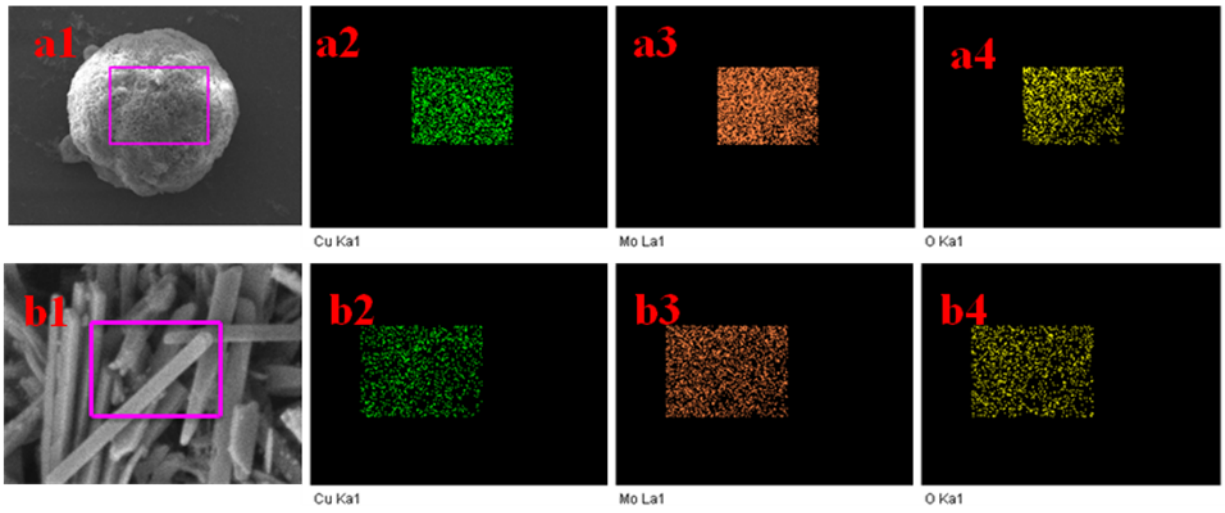

Fig. S16 Area mapping of as-synthesized (a1) prickly sphere and (b1) rod like CMOH microstructures: for the element Cu (a2 and b2), Mo (a3 and b3), and O (a4, and d4).

Scheme S1: Schematic representation of the instrumental set-up for the modified hydrothermal (MHT) method developed in our laboratory.

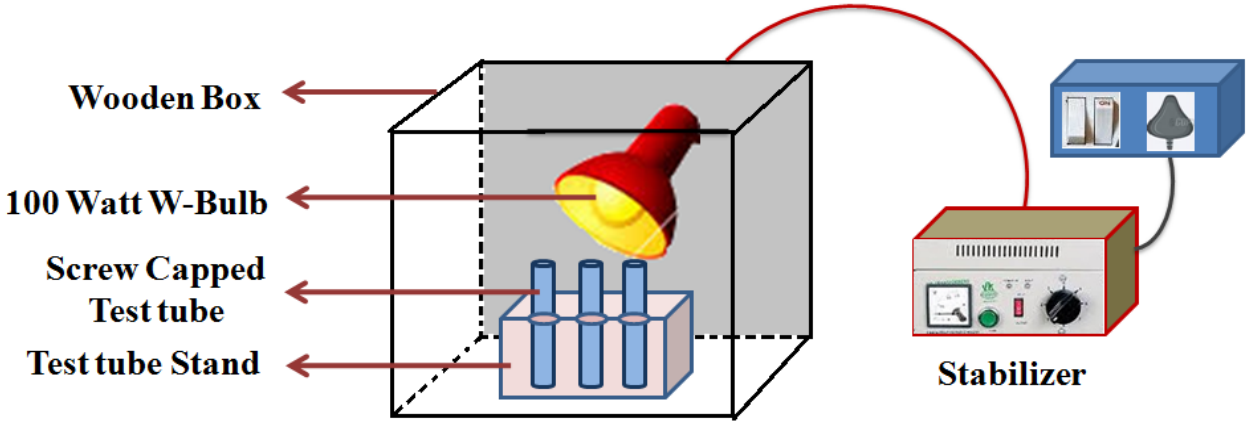

Physical parameters for this experimental set up

1. Screw capped test tube: (a) Length 10.5 cm
   (b) Diameter 1.5 cm
   (c) Volume 15 mL
2. Temperature: 80-90 °C
3. Pressure: Autogenic created inside the screw capped test tube
4. Voltage of electric source: 220 V
5. Wooden box: 6 inch × 6 inch × 7 inch

Table S1: Comparison of photocatalytic dye degradation with different POMs as catalyst.

Catalyst	Congo Red Dye (Concentration)	Condition	Time (min)	Conversion (%)	References
$Na_7PW_{11}O_{39}.nH_2O$-TiO_2 $Na_7PW_{11}O_{39}.nH_2O$-SiO_2 (film)	1 mmol/L	UV light	240	73.2 59.4	57
TiO_2-APS-$PW_{11}Ni$ TiO_2-APS-$PW_{11}Co$ (0.1 g)	50 mg/L	UV light	60	94 93	58
$H_3PW_{12}O_{40}/ZrO_2$ (0.02 g)	20 ppm (10 mL)	UV light, Ultrasonic wave, Optimum pH, O_2 flow rate = 5 mL/min	5	95	55
TiO_2-PVMo (0.05 g)	40 ppm (15 mL)	Visible light, Ultrasonic wave, pH = 4.3, O_2 flow rate = 5 mL/min	20	94	56
$H_3PW_{12}O_{40}/TiO_2$ (0.25 g)	50 mg/L	Visible light	120	92	59
$FeW_{11}O_{39}^{9-}/TiO_2/SiO_2$ (film)	1×10^{-3} mol/L	Visible light, pH = 4	120	68	60
Concave hexagonal ACM (0.01 g)	2×10^{-5} M (50 mL)	Visible light	12	92	In this work

Table S2a: Elemental analysis for differently shaped ACMs.

ACMs	Weight % for Cu	Weight % for Mo	Weight % for N
Calculated	15.15	45.74	6.68
Hexagonal plate	15.09	45.82	6.62
Circular plate	15.21	45.69	6.59
Hollow flower	15.23	45.66	6.72
Concave hexagonal plate	15.06	45.78	6.74

Table S2b: Elemental analysis for differently shaped CMOHs.

CMOHs	Weight % for Cu	Weight % for Mo
Calculated	35.01	35.24
Prickly Sphere	34.94	35.32
Rod	35.05	35.29